Polyvinylidene fluoride multi-scale nanofibrous membrane modified using N-halamine with high filtration efficiency and durable antibacterial properties for air filtration

Weili Shao [a,b,*], Junli Li [a,b], Yuting Zhang [a,b], Ning Sun [a,b], Ting Wu [a,b], Mengmeng Yan [a,b], Fan Liu [a,b,*], Huadong Jiang [c], Xiaogang Chen [a,b], Jianxin He [a,b,*]

[a] Textile and Garment Industry of Research Institute, Zhongyuan University of Technology, Zhengzhou 450007, People's Republic of China
[b] International Joint Laboratory of New Textile Materials and Textiles of Henan Province, Zhengzhou 450007, People's Republic of China
[c] Jiangxi Palm Care Medical Technology Co., LTD, Jiangxi 344399, People's Republic of China

HIGHLIGHTS

- PVDF nanofiber membrane modified by haloamine salt has 99% antibacterial properties against *E. coli* and *S. aureus*.
- The multi-scale PVDF-PAA-TMP-Cl nanofiber films were successfully prepared by depositing ultra-fine (20–35 nm) nanofiber layers on the surface of antibacterial scaffold fiber films.
- After optimizing performance parameters, the multi-scale nanofiber member has excellent filtration efficiency (99.93 %) and low filtration resistance (79pa) for $PM_{0.3}$ and the antibacterial properties of *E. coli* and *S. aureus* were still above 90 % after 10 cycles of chlorination.
- The preparation of multi-scale nanofiber membrane with high efficiency filtration and lasting antibacterial activity provides a new idea for the research of air and water filtration and protective materials.

GRAPHICAL ABSTRACT
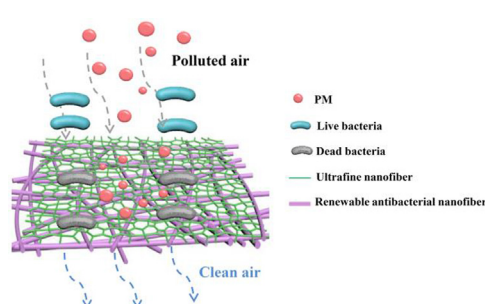
ARTICLE INFO

ABSTRACT

Hypothesis: Particulate matter (PM) pollution and the coronavirus (COVID-19) pandemic have increased demand for protective masks. However, typical protective masks only intercept particles and produce

peculiar odors if worn for extended periods owing to bacterial growth. Therefore, new protective materials with good filtration and antibacterial capabilities are required.

Experiments: In this study, we prepared multi-scale polyvinylidene fluoride (PVDF) nanofibrous membranes for efficient filtration and durable antibacterial properties via *N*-halamine modification.

Findings: The *N*-halamine-modified nanofibrous membrane (PVDF-PAA-TMP-Cl) had sufficient active chlorine content (800 ppm), and the tensile stress and strain were improved compared with the original membrane, from 6.282 to 9.435 MPa and from 51.3 % to 56.4 %, respectively. To further improve the interception efficiency, ultrafine nanofibers (20–35 nm) were spun on PVDF-PAA-TMP-Cl nanofibrous membranes, and multi-scale PVDF-PAA-TMP-Cl nanofibrous membranes were prepared. These membranes exhibited good $PM_{0.3}$ interception (99.93 %), low air resistance (79 Pa), promising long-term $PM_{2.5}$ purification ability, and high bactericidal efficiency (>98 %). After ten chlorination cycles, the antibacterial efficiency against *Escherichia coli* and *Staphylococcus aureus* exceeded 90 %; hence, the material demonstrated highly efficient filtration and repeatable antibacterial properties. The results of this study have implications for the development of air and water filtration systems and multi-functional protective materials.

1. Introduction

Statistics published by the World Health Organization (WHO) show that more than four million premature human deaths are caused annually by the inhalation of fine particles [1–4]. In addition, more than six million people have died owing to the ongoing coronavirus (COVID-19) pandemic [5–8]. Personal protective masks offer the most direct and effective protection in daily life [9–10]. However, most masks produce an odor after extended periods of use and cause physical discomfort as a result of bacterial growth [11–13]. Therefore, it is necessary to develop high-performance mask-filter elements with antibacterial capabilities [14–15].

Melt-blown nonwoven materials are used as core filter layers in masks, and their filtration effect depends on electrostatic adsorption [16]. However, the electrostatic effect is significantly attenuated by environmental factors, such as temperature and humidity, which significantly reduces the filtration efficiency [17]. Nanofibrous materials prepared using electrospinning technology have characteristics such as fine fibers, large specific surface areas, high porosity, and good pore connectivity, which are desirable for air-filtration applications [18–19].

Electrospinning has been used successfully to fabricate nanofibrous membranes from various polymers, such as polyacrylonitrile (PAN) [20], polyamide (PA) [21], polyethylene terephthalate (PET) [22], polyurethane (PU) [23], and polyvinylidene fluoride (PVDF) [24–25], which have been applied to air filtration. In particular, PVDF has been used to construct high-performance particulate matter (PM) filters owing to its excellent chemical inertness, good mechanical properties, thermal stability, and inherent polar structure [26–27].

In previous studies, we constructed multi-scale PVDF nanofibrous membranes comprising scaffold (200 ± 5 nm) and ultrafine nanofibers (20–35 nm) using electrospinning technology, which had a $PM_{0.3}$ capture efficiency of up to 99.92 % and an airflow resistance of 69 Pa [28]. Similarly, Zhang et al. prepared interconnected ultrafine nano-networks (20 nm) via electrospinning/netting, and their results showed a $PM_{2.5}$ capture efficiency of 99.984 % and an airflow resistance of 68 Pa [29]. Furthermore, Liu et al. prepared PVDF nanofiber/net membranes with two-dimensional networks via an innovative in-situ electret electrospinning/netting technique, which exhibited a high $PM_{0.3}$ capture efficiency of 99.998 % and an airflow resistance of 101.325 Pa [30]. However, nanofibrous membrane materials do not have antibacterial properties and cannot kill bacteria rapidly and efficiently; hence, they cannot prevent biological pollution caused by bacterial adhesion [31].

Several studies have shown that metal ions [32–33], quaternary ammonium salts [34], and *N*-halamines [35] can be used to prepare electrospinning nanofibrous membranes with antibacterial properties [36]. Among them, *N*-halamines are commonly used as antibacterial agents owing to their excellent stability, bactericidal effect, reusability, and relatively low cost [37]. Moreover, *N*-halamines can be immobilized on the membrane surface via copolymerization, grafting, blending, and coating to achieve antibacterial functionalization [38]. Liang et al. prepared polyvinyl alcohol nanofibers via electrospinning and then soaked the fibers in an *N*-halamine compound (dimethylol-5,5-dimethylhydantoin) to achieve covalent grafting [39]. The modified nanofibrous membranes were rechargeable, demonstrated long-lasting antibacterial properties, and had high bacterial-inactivation efficiency (>99 %). Wang et al. prepared a $PVDF/SiO_2$ ultrafiltration membrane based on *N*-halamine-functionalized SiO_2 nanospheres and embedded SiO_2 microspheres via non-solvent immersion phase separation, which has the highest sterilization efficiency against *Escherichia coli* (*E. coli*) and *Staphylococcus aureus* (*S. aureus*) (up to 97.1 % and 97.0 %, respectively) [40]. Capakova et al. successfully prepared an antibacterial PVDF/dodecyltrimethylammonium bromide (DTAB) membrane for air filtration using a one-step electrospinning method, where an antibacterial agent was added to a spinning solution, which completely inhibited the growth of gold *S. aureus* [41].

This study presents a method of fabricating multi-scale nanofibrous membranes with antibacterial functions and high filtration efficiency. Scaffold PVDF nanofibers (200 ± 10 nm) are used as the substrate. Thereafter, the *N*-halamine precursor PVDF-polyacrylic acid (PAA)-2,2,6,6-tetramethyl-4-piperidinol (TMP) containing a *N*-X bond is obtained via chemical reaction. Next, scaffold PVDF-PAA-TMP-Cl nanofibers with repeatable antibacterial function are obtained via chlorination. Finally, ultrafine PVDF nanofibers (20–35 nm) are spun using PVDF-PAA-TMP-Cl scaffold nanofibers as a substrate to obtain nanofibrous materials with high air-filtration efficiency and antibacterial function. The $PM_{0.3}$ filtration performance, antibacterial function, and repeatable antibacterial effect on *E. coli* and *S. aureus* of the multi-scale nanofibrous membrane are discussed. Therefore, a new strategy for fabricating nanofibrous materials based on modified PVDF with repeatable antibacterial activity and high-precision filtration is proposed.

2. Materials and methods

2.1. Materials and reagents

PVDF (M_w = 300,000 and M_w = 600,000) were purchased from Bayer, Germany. *N,N*-dimethylformamide (DMF), tetrabutylammonium chloride (TBAC), sodium hydroxide (NaOH), potassium permanganate ($KMnO_4$), sodium bisulfite ($NaHSO_3$), sulfuric acid

(H$_2$SO$_4$), p-toluenesulfonic acid (C$_7$H$_8$O$_3$S), potassium hydrogen sulfate (KHSO$_4$), sodium hypochlorite (NaClO), and sodium thiosulfate (Na$_2$S$_2$O$_3$), and potassium iodide (KI) were purchased from China Xi long Science Co., ltd. TMP and PAA (M_w = 10,000) were purchased from Macklin Co., ltd. *E. coli* ATCC29522 and *S. aureus* ATCC29523 were purchased from Henan Huibo Medical Co., ltd. All chemicals were analytically pure and used without further purification.

2.2. Preparation of PVDF-PAA-TMP-Cl nanofibrous membrane

Nanofibers prepared by electrospinning is shown in Fig. 1a and the PVDF scaffold nanofibers were prepared in a spinning solution of 20 wt% TBAC and 0.7 wt% PVDF (M_w = 300,000). The prepared PVDF scaffold nanofibrous membrane was immersed in a 3 % NaOH solution with 5 wt% KMnO$_4$ and reacted at 58 °C for 30 min for defluorination. Subsequently, it was washed with deionized water and immersed in 5 wt% H$_2$SO$_4$ solution with 3 % NaHSO$_3$ for 30 min at room temperature (~25 °C) to obtain a hydroxylated PVDF nanofibrous membrane (Fig. 2a). Thereafter, the nanofibrous membrane was immersed in 15 wt% PAA solution, reacted at 50 °C for 2 h, washed with deionized water, and dried at 40 °C for 2 h to obtain a PVDF-PAA nanofibrous membrane (Fig. 2b). To prepare the 2 wt% TMP solution, C$_7$H$_8$O$_3$S and potassium bisulfate were added to the solution, and the dried PVDF-PAA nanofibrous membrane was immersed in the solution and reacted at 120 °C for 2 h to obtain the *N*-halamine precursor PVDF-PAA-TMP nanofibrous membrane. Finally, the PVDF-PAA-TMP nanofibrous membrane was immersed in NaClO solution with 3000 ppm active chlorine content to achieve chlorination and reacted at room temperature for 45 min to obtain a PVDF-PAA-TMP-Cl nanofibrous membrane with antibacterial function (Fig. 2c).

2.3. Preparation of multi-scale PVDF-PAA-TMP-Cl nanofibrous membranes

PVDF-PAA-TMP-Cl nanofibers were used as the receiving substrate to generate ultrafine PVDF nanofibers using electrospinning equipment. The ultrafine nanofibers were prepared in a spinning solution of 5 wt% TBAC and 3 wt% PVDF (M_w = 600,000), and a PVDF-PAA-TMP-Cl nanofibrous membrane with a multi-scale structure was obtained.

2.4. Filtration performance test

The filtration performance of nanofibrous membranes at different airflow rates was evaluated using a TSI 8130A automatic filter-

material tester. Each sample was cut into a circle with a diameter of approximately 15 cm; the tests were repeated five times for each sample, and the average value was calculated. The filtration efficiency and pressure reduction were calculated using the equations [42]:

$$\eta = \frac{C_{in} - C_{out}}{C_{in}} \times 100\% \tag{1}$$

and

$$\Delta P = P_{in} - P_{out} \tag{2}$$

where η is the filtration efficiency; C_{in} and C_{out} represent the particle concentrations upstream and downstream from the filter, respectively; ΔP is the filter pressure decrease; P_{in} and P_{out} represent the pressure upstream and downstream from the filter, respectively.

The equation used to calculate the quality factor, expressed by Q_f, was [43]:

$$Q_f = \frac{-In(1 - \eta)}{\Delta P} \tag{3}$$

2.5. Chlorination and reactive chlorine content testing

Different weights of PVDF-PAA-TMP-Cl nanofibrous membranes were placed in a beaker and submerged in 40 mL of deionized water. Subsequently, 0.4 g of KI was added, dissolved in 10 mL of aqueous starch solution (1 wt%), and stirred with a glass rod for 10 min to obtain a purple solution. Finally, Na$_2$S$_2$O$_3$ solution was added quantitatively with a pipette for reduction. When the solution became colorless, the content was recorded. Each experiment was repeated five times under the same conditions, and the average value was calculated. The equation used to calculate the chlorine content was [44]:

$$Cl^+\% = \frac{N \times V \times 35.45}{2M} \times 100 \tag{4}$$

where N represents the concentration of Na$_2$S$_2$O$_3$ solution (equiv/L); V represents the volume (L) of Na$_2$S$_2$O$_3$ solution added, and M represents the weight (g) of the PVDF-PAA-TMP-Cl nanofibrous membrane.

2.6. Antibacterial performance test

The antibacterial efficiency of the nanofibrous membrane was measured using a plate colony count method. First, solutions of *E. coli* and *S. aureus* were shaken evenly and diluted sequentially
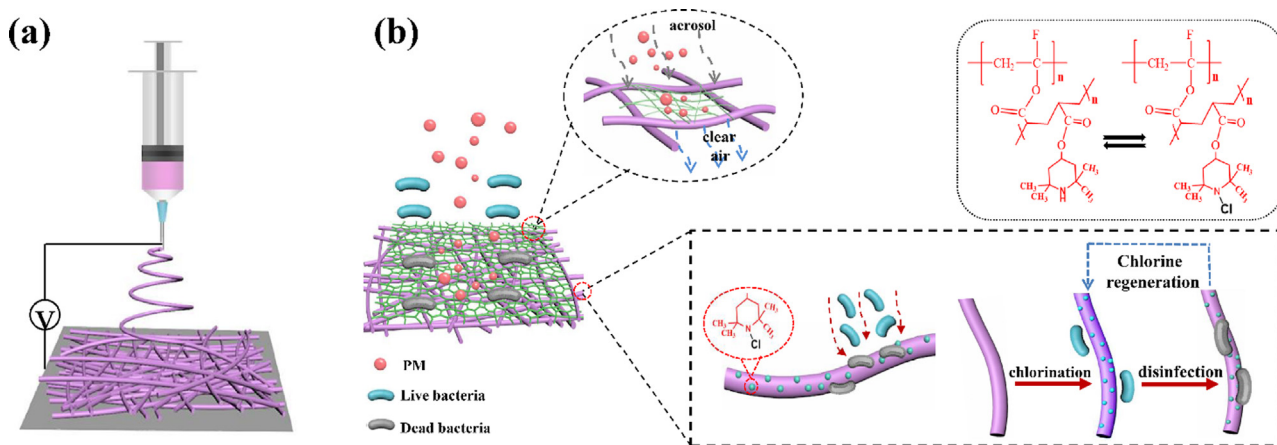

Fig. 1. (a) Schematic showing the electrospinning. (b) Design and renewable antibacterial function of multi-scale PVDF-PAA-TMP-Cl nanofibrous membrane.
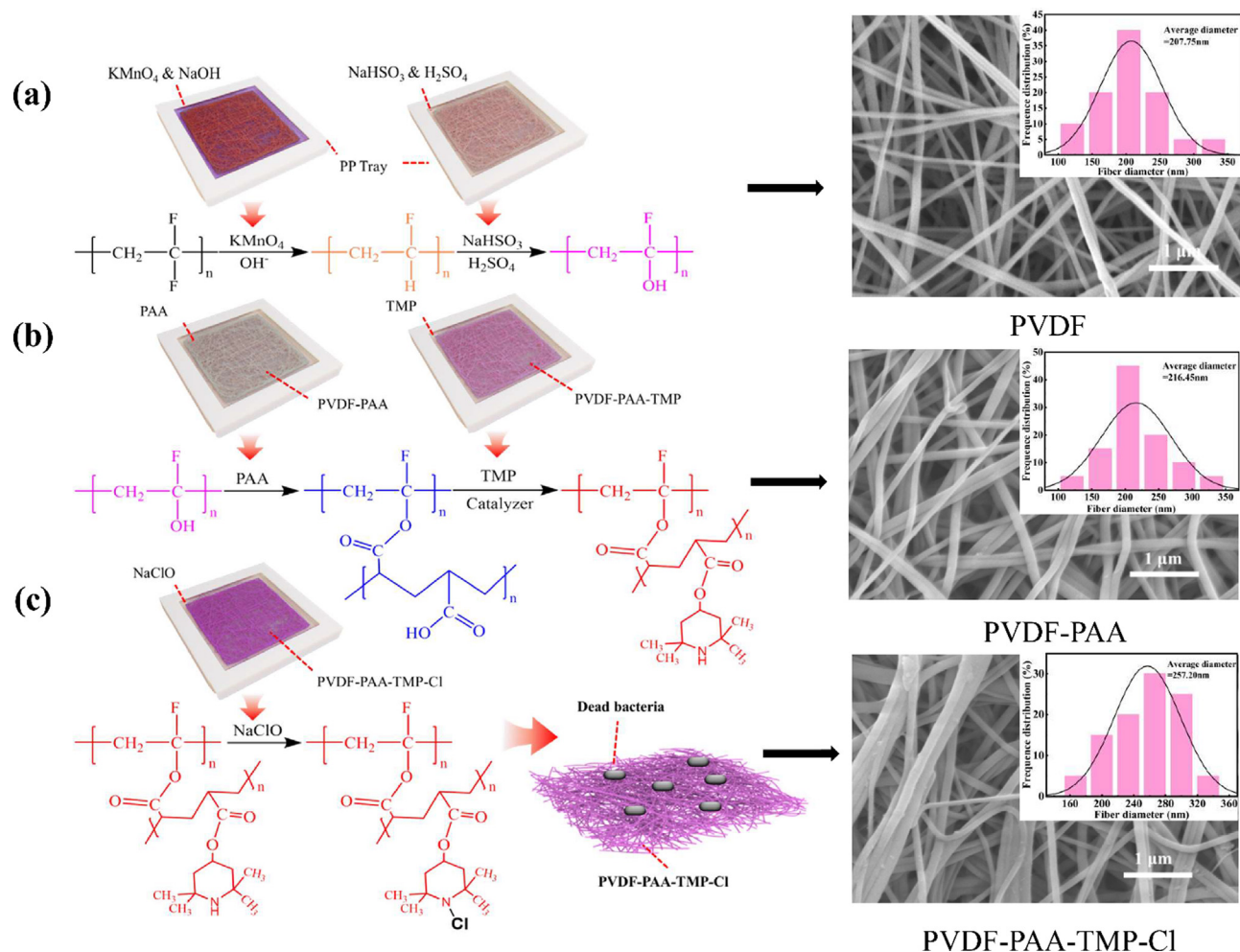
Fig. 2. *N*-halamine modification process and corresponding FE-SEM images. (a) Hydroxylation modification, (b) hydroxyl esterification, and (c) chlorination reaction.

in the corresponding buffer until the colonies were diluted to 10^6 CFU/mL. The blank control group and groups with different weights (0.5, 1, and 1.5 g m^{-2}) of PVDF-PAA-TMP-Cl nanofibrous membranes (measuring 2×2 cm^2) were placed on a 24-well plate and labeled B-1, P-1, P-2, and P-3, respectively. Thereafter, 200 µL of 10^6 CFU/mL bacterial solution was added to the wells using a pipette. The plate was sealed and placed in an incubator at a constant temperature (37 °C) for 3 h. The bacterial liquid was removed from the samples and diluted 1000 times with buffer solution. Finally, 100 µL of each bacterial liquid was coated on a solid medium plate and sealed. The plates were placed in an incubator at a constant temperature (37 °C) for 12 h. Afterward, the number of colonies on each plate was counted. Each experiment was repeated five times under the same conditions, and the average value was calculated. The antibacterial rate was calculated using the equation [45]:

$$\text{Antibacterial rate}\,(\%) = \frac{Mb - Ms}{Mb} \times 100\% \qquad (5)$$

where M_s and M_b are the numbers of bacteria after incubating a specimen and blank sample, respectively.

2.7. Characterization

The morphology of the nanofibrous membrane was observed using scanning electron microscopy (SEM Phenom Pure, Netherlands Electronics Company, Netherlands) and field-emission scan-ning electron microscopy (FE-SEM FEI SIRION-100, Shanghai Funa Scientific Instrument Co., ltd., China). The strength of the films was evaluated using a tensile strength tester (XLW (EC)-a, Languang Electromechanical Technology Co., China). The pore size was analyzed using a high-performance automatic mercury porosimeter (Autopore IV 9500, Micromeritics, USA). The chemical elements were detected using Fourier-transform infrared (FT-IR) spectroscopy with a scan range of 400–4000 cm^{-1} (Nicolet 6700, Thermo-Fisher Co., ltd., USA). The elements and chemical bonds were analyzed using X-ray photoelectron spectroscopy (XPS; K-Alpha, Thermal VG Company, UK.).

3. Results and discussion

3.1. Design of the multi-scale PVDF-PAA-TMP-Cl nanofibrous membrane and repeatable antibacterial function

Multi-scale PVDF nanofibrous membranes with long-lasting antibacterial function were prepared in three stages: (1) a PVDF scaffold nanofibrous membrane with good fiber morphology was prepared via electrospinning; (2) *N*-halamine was grafted onto the scaffold nanofibrous membranes to obtain PVDF-PAA-TMP-Cl nanofibrous membranes with antibacterial function; (3) high-efficiency and low-resistance filtration nanofibrous materials with renewable antibacterial functions were fabricated by electrospin-ning PVDF ultrafine nanofibers on reproducibly chlorinated PVDF-PAA-TMP-Cl nanofibrous membranes.

The preparation of the multi-scale PVDF-PAA-TMP-Cl renewable antibacterial nanofibrous membranes is shown in Fig. 1. The nanofibrous membranes were prepared via electrospinning, and the structure of the nanofibers, including the diameter of the fibers and pore size distribution, was controlled by changing the electrospinning parameters. A cyclic chlorination experiment was designed to confirm the regenerative function of active chlorine. After chlorination, the N—H group in the modified PVDF was converted to a bactericidal *N*-Cl group, and the *N*-Cl group was regained after re-chlorination to provide repeated antibacterial function.

3.2. Structural characterization of PVDF-PAA-TMP-Cl nanofibrous membrane

Fig. 2 shows the process used to modify the PVDF scaffold nanofibrous membrane and corresponding nanofibrous electron microscope images. The FE-SEM results shown in Fig. 2 (a–c) reveal that morphology of the PVDF nanofibers was unaffected when the material was soaked in strong acid, alkali, or strong oxidizing solutions, which was attributed to the good chemical stability of PVDF [45]. However, the PVDF nanofibers changed from the initial single fibers to the subsequent multiple cross-linked fibers, particularly after chlorination, and the average fiber diameter increased from 207 to 257 nm. This phenomenon may increase the pore size and widen the pore-size distribution of the nanofibrous membrane, which are not conducive to the interception of particles. Therefore, in subsequent studies, we will spin ultrafine PVDF nanofibers based on PVDF-PAA-TMP-Cl to try and mitigate the pore size issue and rely on ultrafine PVDF nanofibrous membranes to intercept particles, improve filtration efficiency, and achieve the purpose of antibacterial and efficient filtration.

3.3. Surface morphology and elemental composition of modified PVDF fiber

To observe the overall morphology of the chlorinated PVDF nanofibrous membrane in more detail, the nanofibers were observed at various resolutions, as shown in Fig. 3a–c. The low-magnification ($\times$2000) image of the nanofibrous membrane revealed good overall morphology. The partially enlarged ($\times$50,000) and ($\times$150,000) images showed that the fiber exhibited a regular and smooth morphology. Therefore, the modified PVDF nanofibrous membrane was not damaged and could be re-used.

To verify the successful chlorination of PVDF nanofibers, the surface elements of the fibers were analyzed by Mapping and EDS of FE-SEM. The distributions of C, F, N, and Cl are shown in Fig. 3d. The preliminary assessment was that the modified PVDF nanofibers contained *N*-halamine groups (*N*-Cl). As shown in Fig. 3e–f, before modification, the EDS analysis showed characteristic peaks corresponding to C and F, representing 52.82 % and 46.79 % of the total content, respectively. However, after modification characteristic peaks corresponding to O, N, and Cl were also present, representing 2.03 %, 1.35 %, and 1.21 % of the total content, respectively. These results demonstrate that PVDF nanofibers were successfully grafted using TMP and a chlorination reaction.

The *N*-halamine group (*N*-Cl) in the modified PVDF nanofiber affected the antibacterial effect. We analyzed the PVDF before and after chlorination using FT-IR spectroscopy and XPS. As shown in Fig. 3g, compared with the original membrane, the PVDF-PAA-TMP nanofibrous membrane had more distinct characteristic absorption peaks at 3300, 2846, 1740, and 1667 cm^{-1}. The peak at 3300 cm^{-1} was the stretching vibration peak of –OH, which was mostly formed by the "dehydrofluorination" of PAA and PVDF [46]. The peak at 2846 cm^{-1} was a characteristic absorption peak corresponding to the –CH$_2$ in TMP [47]. The most important con-

sideration for the chlorinated PVDF nanofibrous membrane was whether the *N*-X bond transformed to the *N*-Cl bond. As shown in Fig. 3h, the characteristic peaks of the PVDF-PAA-TMP-Cl nanofibrous membranes at 2846 and 1740 cm^{-1} were shifted. The peak at 2846 cm^{-1} shifted to 2855 cm^{-1}, which was mostly attributed to the shift in the adjacent –CH$_3$ bond owing to the electrophilic induction effect of chlorinated *N*-Cl [47]. The peak at 1740 cm^{-1} shifted to 1745 cm^{-1} and broadened. In general, the *N*-halamine compounds containing carbon groups will shift to higher wavenumbers after chlorination [48–49]. These phenomena prove that the *N*-H in TMP was successfully transformed into *N*-Cl.

The XPS results (Fig. 3i–j) show that the PVDF-PAA-TMP-Cl nanofibrous film had additional Cl 2p peaks at 200.80 eV. According to the peak fitting of high-resolution Cl 2p fine spectrum, Cl 2p existed in four states: *N*-Cl 2p1/2, *N*-Cl 2p3/2, Cl 2p1/2, and Cl 2p3/2 at 201.5, 200.2, 199.6, and 198.8 eV, respectively [50–51]. These results demonstrate that the grafting reaction and chlorination were successful.

The mechanical properties of the modified scaffold PVDF nanofibrous membranes were related to the subsequent formation of multi-scale structures and the stability of the filtration efficiency. Fig. 3k shows that the tensile stress of the PVDF-PAA-TMP-Cl nanofibrous membrane was better than that of the unmodified membranes, with a stress of 9.435 MPa and strain of 56.4 %. This may be because the mutual crosslinking between the fibers increases the cohesive force between the nanofibers; therefore, tensile stress is evenly dispersed, which effectively improves the tensile breaking strength of the membrane [52].

3.4. Analysis of the antibacterial properties of PVDF-PAA-TMP-Cl nanofibrous membranes

Considering the balance between the antibacterial performance and subsequent filtration performance, PVDF-PAA-TMP-Cl nanofibrous membranes with different weights (P-1, P-2, and P-3) were prepared, and their active chlorine content and antibacterial performance were explored. Fig. 4a shows the change in the active chlorine content of the PVDF-PAA-TMP-Cl nanofibrous membrane with chlorination time. Two distinct characteristic regions were observed. In the first hour, rapid linear chlorination was observed, which was followed by a saturation region, wherein the chlorine content increased slowly. After 1 h of chlorination, the active chlorine contents of the P-1, P-2, and P-3 samples were 550, 725, and 800 ppm, respectively; after 6 h of chlorination, the saturated contents were 570, 766, and 832 ppm (P-3), respectively. These results show that the chlorine content of PVDF-PAA-TMP-Cl increased as the weight of the PVDF increased. During the reaction, the quantity of PVDF nanofiber participating in the reaction increased, and more active sites were generated. Therefore, the resulting PVDF-PAA-TMP had more *N*-X bonds to participate in chlorination and obtain *N*-Cl bonds; hence, the active chlorine content was higher.

To gain insight into the chlorination process, we investigated the relationship between the chlorination pH and chlorine content for pH values between 2 and 12. As shown in Fig. 4b, chlorination was highly dependent on pH, and the efficiency was highest when the pH was approximately 6 [53]. The PVDF membranes only reached a low chlorine content of < 400 ppm under acidic or alkaline conditions.

As shown in Fig. 4c–d, samples P-1, P-2, and P-3 killed 2 log, 4 log, and 5 log CFU of *E. coli* and *S. aureus,* respectively, within 30 min. The results in Fig. 4e–f show that the low-weight sample P-1 had a low active chlorine content, and the antibacterial efficiency against *E. coli* and *S. aureus* was higher than 80 %, whereas the higher-weight samples P-2 and P-3 had higher active chlorine contents, and their antibacterial efficiency was higher than 98 %, indicating excellent antibacterial performance. Consistent with
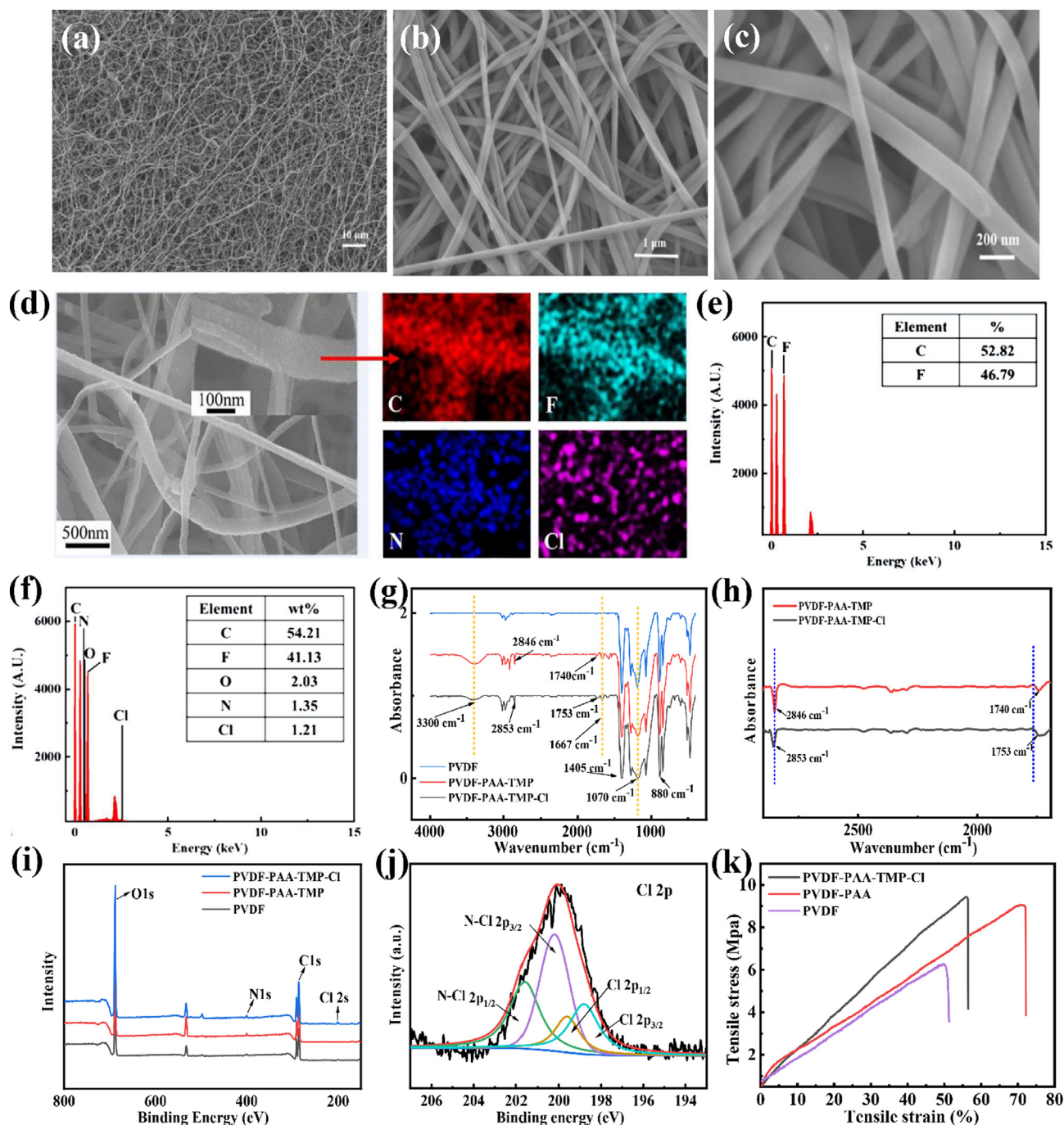
Fig. 3. FE-SEM image of chlorinated PVDF nanofibrous membranes at (a) × 2000, (b) × 50,000, and (c) × 150,000 magnifications. (d) FE-SEM images and elemental mapping of PVDF-PAA-TMP-Cl at different scales. EDS images of (e) PVDF and (f) PVDF-PAA-TMP-Cl. (g) FT-IR images of PVDF and PVDF-PAA-TMP before and after chlorination. (h) Shift of two infrared absorption peaks of PVDF-PAA-TMP before and after chlorination. (i) XPS spectra. (g) XPS fitting curves of *N*-Cl and Cl 2p. (k) Mechanical properties.

the previous chlorination experiments, the antibacterial performance was directly dependent on the weight of the nanofibrous membrane.

3.5. Analysis of the filtration performance of the multi-scale PVDF-PAA-TMP-Cl nanofibrous membrane

To determine the relative balance between filtration performance and antibacterial efficiency, the ultrafine PVDF nanofibers were spun on the surface of PVDF-PAA-TMP-Cl nanofibers (P-1, P-2, and P-3) with different weights to improve their filtration performance. Based on a previous study, the PVDF ultrafine fiber layer

was re-spun to 0.5 ± 0.12 g m^{-2} [28]. As shown in Fig. 5a, the pore size distributions of the P-1, P-2, and P-3 samples were concentrated as the weight increased, and the average pore sizes were 3.86, 2.35, and 1.98 μm for P-1, P-2, and P-3, respectively. This is because the nanofibers were more densely packed as the weight of the membrane increased. Accordingly, after spinning the microfiber layer, the pore structure was further improved owing to the contribution of the microfiber layer, and the average pore sizes were reduced to 1.15, 0.69, and 0.66 μm for P-S1, P-S2, and P-S3, respectively. Although the size of the pores between the fibers decreased, the porosity of the corresponding fiber membrane did not change significantly (Fig. 5b). The results show that ultrafine
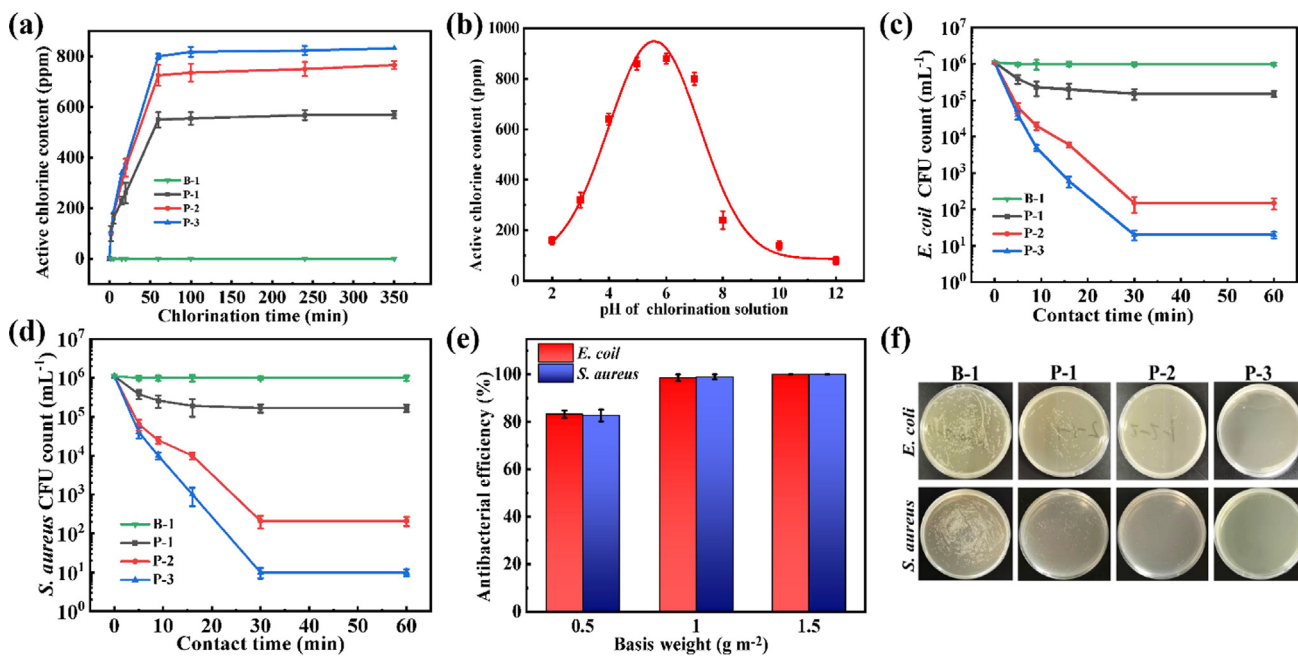
Fig. 4. (a) Active chlorine content of P-1, P-2, and P-3; (b) change in the active chlorine content of P-2 versus pH of chlorination solutions. Bactericidal activity of different membranes against (c) *E. coli* and (d) *S. aureus*. (e) Antibacterial efficiency and (f) photographs of *E. coli* and *S. aureus* culture plates with different samples.
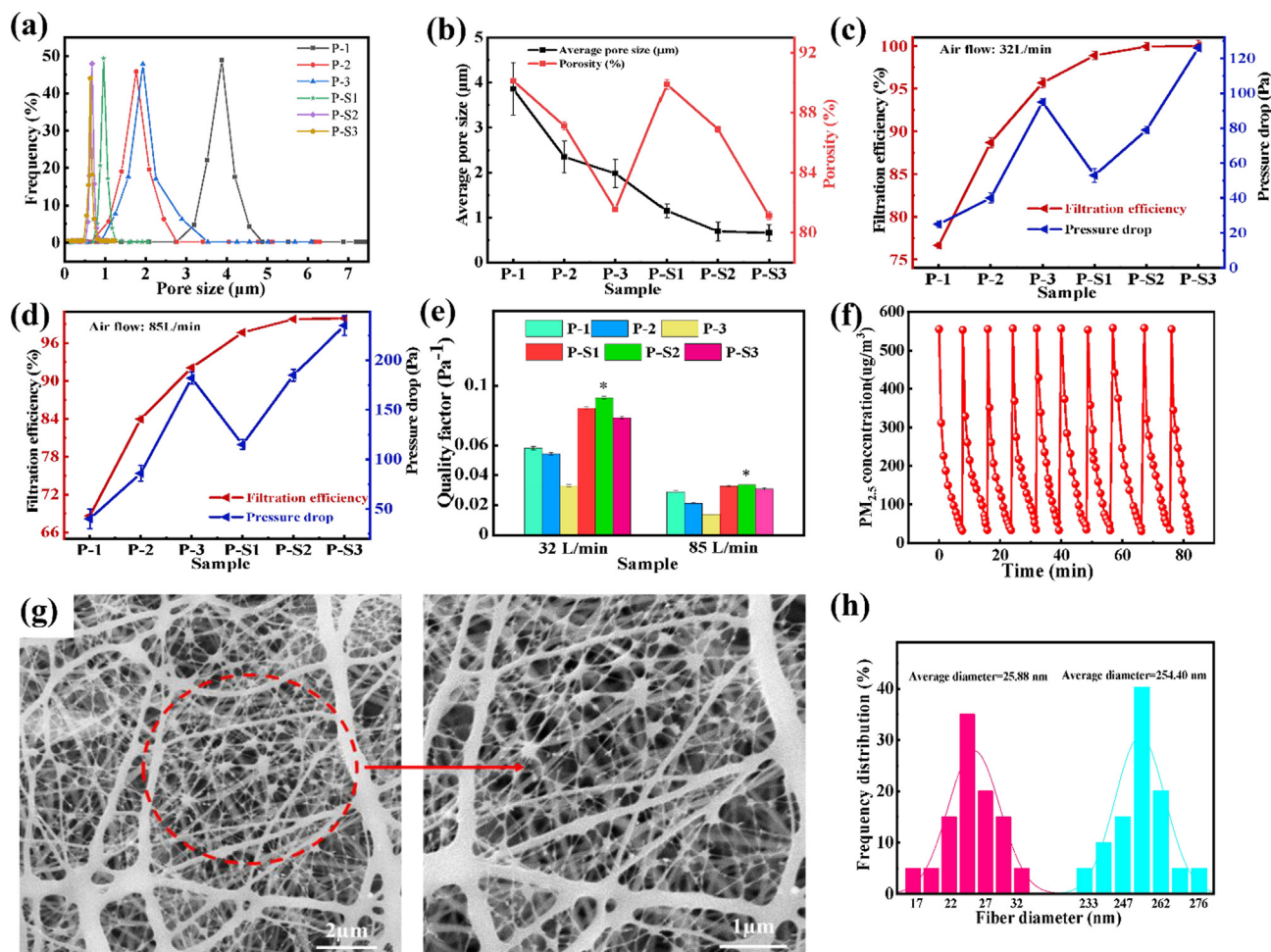

Fig. 5. Pore structures of P-1–P-S3: (a) pore-size distribution and (b) average pore size and porosity. PM$_{0.3}$ NaCl filtration performance of P-1–P-S3 with airflow rates of (c) 32 L/min and (d) 85 L/min. (e) Quality factor for different samples. Analysis of P-S2: (f) long-term recycling performance for removing PM$_{2.5}$; (g) SEM images; (h) fiber-diameter distribution.
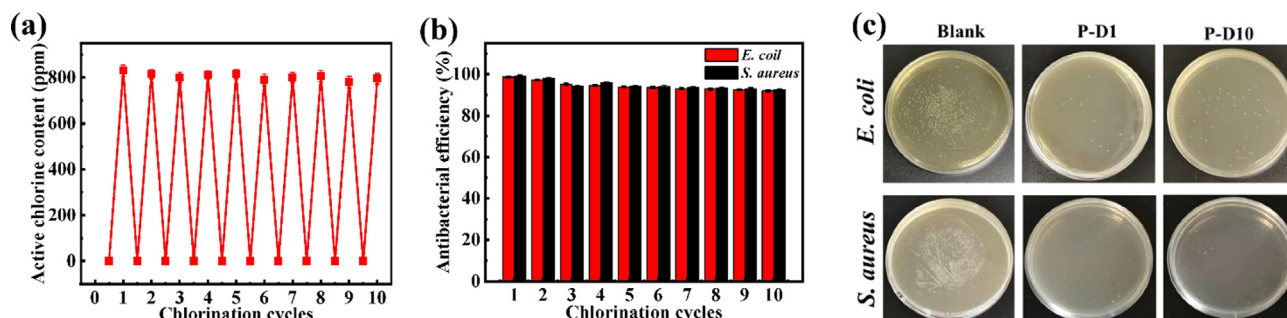
Fig. 6. (a) Ten cyclic chlorination tests; (b) ten cycle rechargeable biocidal test of P-S2 against *E. coli* and *S. aureus*; (c) colony growth of *E. coli* and *S. aureus* over ten cycles.

PVDF nanofibers alleviated the issue of large average pore sizes in PVDF-PAA-TMP-Cl nanofibrous membranes, but they did not increase the bulk density. Therefore, the ability of the membrane to intercept airborne particles was improved without a significant increase in air resistance.

The $PM_{0.3}$ filtration efficiency was tested at different flow rates, and the results are shown in Fig. 5c–e. The quality factors gradually decreased from P-1 to P-3 (Fig. 5e), owing to the increase in the weight of the membrane and the packing density of the nanofibers. Although the pore size decreased, a significant reduction in porosity was observed. However, spinning ultrafine PVDF nanofibers in the PVDF-PAA-TMP-Cl nanofibrous membranes significantly improved the filtration efficiency. At an airflow rate of 32 L/min (Fig. 5c), the filtration efficiencies increased from 76.65 %, 88.68 %, and 95.68 % for P-1, P-2, and P-3, respectively, to 98.89 %, 99.93 %, and 99.995 % for P-S1, P-S2, and P-S3, respectively. Moreover, the pressure drops increased slightly, from 28, 35, and 39 Pa for P-1, P-2, and P-3, respectively, to 53, 79, and 126 Pa for P-S1, P-S2, and P-S3, respectively. Owing to the support of the microfiber layer, the quality factor was significantly improved. Notably, the filtration efficiency of P-S2 remained above 99.8 % at an airflow rate of 85 L/min (Fig. 5d), and the quality factor was highest at airflow rates of 32 and 85 L/min and were 0.092 and 0.0338 Pa^{-1}, respectively (Fig. 5e). This is because the filtration performance of the fiber membrane was closely related to the pore structure, and increasing the membrane weight resulted in tighter packing between fibers, which increased the filtration resistance. Significantly, P-S2 simultaneously possessed a small pore size (0.69 μm), high porosity (87.10 %), interconnected pore structure, and good fiber morphology (Fig. 5g–h), indicating that it is well suited for air filtration.

The long-term cycling air-purification efficiency is an important aspect of filtration performance. Therefore, we investigated the cycle purification performance of P-S2. As shown in Fig. 5f, after ten purification cycles, the fiber membrane was able to reduce the $PM_{2.5}$ concentration in a 1 m^2 confined space from 555 μg/m^3 (severe pollution) to 38 μg/m^3 (mild pollution) within 10 min. This is consistent with the initial purification capacity and indicates the long-term stability of the filtration performance.

3.6. Analysis of repeatable antibacterial properties of the multi-scale PVDF-PAA-TMP-Cl nanofibrous membrane

To verify that the prepared multi-scale PVDF-PAA-TMP-Cl nanofibrous membrane had the renewable antibacterial properties of *N*-halamine compounds, we tested its antibacterial effects using *E. coli* and *S. aureus* after multiple chlorination steps using P-S2 as a representative sample. The samples were labeled P-D1...P-D10 according to the number of chlorination steps. The results are shown in Fig. 6a. The active chlorine content was reasonably stable over ten chlorination cycles, which was attributed to the good

nanofibrous structure and the stability of the grafted *N*-halamine. As shown in Fig. 6b and c, after two chlorination cycles, the antibacterial effect of the multi-scale PVDF-PAA-TMP-Cl nanofibrous membrane was above 97 % (down from 98 %); after four cycles, it was above 95 %, and after ten cycles, it was above 90 %. This indicates that the multi-scale PVDF-PAA-TMP-Cl nanofibrous membrane possessed reproducible antibacterial properties.

4. Conclusions

A multi-scale nanofibrous membrane with efficient PM removal performance and durable antibacterial properties was prepared. The halamine-modified PVDF scaffold nanofibrous membrane contained sufficient active chlorine (800 ppm) and had an antibacterial efficiency of 99.9 % against *E. coli* and *S. aureus*. To further improve the filtration efficiency, an ultra-fine (20–35 nm) fiber layer was electrospun on the surface of the PVDF-PAA-TMP-Cl nanofibrous membrane. Testing at an airflow rate of 32 L/min revealed that the $PM_{0.3}$ removal efficiency was 99.93 %, and the filtration resistance was 79 Pa. Although many methods of imparting antibacterial properties to polymers, such as PVA [54], PAN [55], and PU [56] have been reported, relatively few reports have considered the antibacterial modification of PVDF halamine regeneration. In this study, a PVDF-PAA-TMP-Cl nanofibrous membrane possessing the reproducible antibacterial function of halamine was successfully prepared via surface chemical modification and surface chemical grafting. The nanofibrous membrane exhibited >90 % antibacterial efficiency against *E. coli* and *S. aureus* after ten chlorination cycles. Therefore, multi-scale PVDF-PAA-TMP-Cl nanofibrous membranes can realize the synergistic effect of high-efficiency filtration and stable and long-lasting antibacterial action, which are of significant significance to the development of air and water filtration systems and multi-functional protective materials.

CRediT authorship contribution statement

Weili Shao: Investigation, Methodology, Funding acquisition, Data curation, Writing - original draft, Writing - review & editing. **Junli Li:** Investigation, Methodology, Validation, Writing - original draft, Writing - review & editing. **Yuting Zhang:** Investigation, Validation. **Ning Sun:** Investigation, Data curation. **Ting Wu:** Investigation, Formal analysis. **Mengmeng Yan:** Validation. **Fan Liu:** Methodology, Resources, Supervision. **Huadong Jiang:** Conceptualization, Methodology, Supervision. **Xiaogang Chen:** Methodology, Supervision, Resources. **Jianxin He:** Conceptualization, Formal analysis, Funding acquisition.

Data availability

Data will be made available on request.

Declaration of Competing Interest

The authors declare that they have no known competing financial interests or personal relationships that could have appeared to influence the work reported in this paper.

Acknowledgements

References

[1] T.T. Bui, M.K. Shin, S.Y. Jee, D.X. Long, J. Hong, M.G. Kim, Ferroelectric PVDF nanofiber membrane for high-efficiency $PM_{0.3}$ air filtration with low air flow resistance, Colloid. Surface. A. 640 (2022), https://doi.org/10.1016/j.colsurfa.2022.128418 128418.

[2] Y. Zhou, Y. Liu, M. Zhang, Z. Feng, D.G. Yu, K. Wang, Electrospun nanofiber membranes for air filtration: a review, Nanomaterials 12 (7) (2022) 1077, https://doi.org/10.3390/nano12071077.

[3] Z. Yang, X. Zhang, Z. Qin, H. Li, J. Wang, G. Zeng, C. Liu, J. Long, Y. Zhao, Y. Li, G. Yan, Airflow synergistic needleless electrospinning of instant noodle-like curly nanofibrous membranes for high-efficiency air filtration, Small 18 (14) (2022) 2107250, https://doi.org/10.1002/smll.202107250.

[4] Y. Liu, C. Jia, H. Zhang, H. Wang, P. Li, L. Jia, F. Wang, P. Zhu, H. Wang, L. Yu, F. Wang, L. Wang, X. Zhang, Y. Sun, B. Li, Free-standing ultrafine nanofiber papers with high $PM_{0.3}$ mechanical filtration efficiency by scalable blow and electro-blow spinning, ACS Appl. Mater. Inter. 13 (29) (2021) 34773–34781, doi: 10.1021/acsami.1c04253.

[5] C.-C. Lai, T.-P. Shih, W.-C. Ko, H.-J. Tang, P.-R. Hsueh, Severe acute respiratory syndrome coronavirus 2 (SARS-CoV-2) and coronavirus disease-2019 (COVID-19): the epidemic and the challenges, Int. J. Antimicrob. Ag. 55 (3) (2020) 105924, https://doi.org/10.1016/j.ijantimicag.2020.105924.

[6] J. Wan, X. Wang, S. Su, Y. Zhang, Y. Jin, Y. Shi, K. Wu, J. Liang, Digestive symptoms and liver injury in patients with coronavirus disease 2019 (COVID-19): a systematic review with meta-analysis, JGH Open. 4 (6) (2020) 1047–1058, https://doi.org/10.1002/jgh3.12428.

[7] H. Li, H. Li, Z. Ding, Z. Hu, F. Chen, K. Wang, Z. Peng, H. Shen, Spatial statistical analysis of Coronavirus Disease 2019 (COVID-19) in China, Geospat, Health 15 (1) (2020), https://doi.org/10.4081/gh.2020.867.

[8] D. Peng, J. Qian, L. Wei, C. Luo, T. Zhang, L. Zhou, Y. Liu, Y. Ma, F. Yin, COVID-19 distributes socially in China: a Bayesian spatial analysis, PLoS ONE 17 (4) (2022), https://doi.org/10.1371/journal.pone.0267001 e0267001.

[9] Y. Xu, X. Zhang, X. Hao, D. Teng, T. Zhao, Y. Zeng, Micro/nanofibrous nonwovens with high filtration performance and radiative heat dissipation property for personal protective face mask, Chem. Eng. J. 423 (2021), https://doi.org/10.1016/j.cej.2021.130175 130175.

[10] A.A. Jazie, A.J. Albaaji, S.A. Abed, A review on recent trends of antiviral nanoparticles and airborne filters: special insight on COVID-19 virus, Air. Qual. Atmos. Hlth. 14 (11) (2021) 1811–1824, https://doi.org/10.1007/s11869-021-01055-1.

[11] E. Atangana, A. Atangana, Facemasks simple but powerful weapons to protect against COVID-19 spread: can they have sides effects?, Results Phys 19 (2020), https://doi.org/10.1016/j.rinp.2020.103425 103425.

[12] L. Liao, W. Xiao, M. Zhao, X. Yu, H. Wang, Q. Wang, S. Chu, Y. Cui, Can N95 Respirators be reused after disinfection? How many times?, ACS Nano 14 (5) (2020) 6348–6356, https://doiorg/10.1021/acsnano.0c03597.

[13] J. Xu, X. Xiao, W. Zhang, R. Xu, S. C. Kim, Y. Cui, T. T. Howard, E. Wu, Y. Cui, Air-filtering masks for respiratory protection from $PM_{2.5}$ and pandemic pathogens, One Earth 3 (5) (2020) 574–589, doi: 10.1016/j.oneear.2020.10.014.

[14] E.A. Ogbuoji, A.M. Zaky, I.C. Escobar, Advanced research and development of face masks and respirators pre and post the coronavirus disease 2019 (COVID-19) pandemic: a critical review, Polymers-Basel 13 (12) (2021) 1998, https://doi.org/10.3390/polym13121998.

[15] C. Tian, F. Wu, W. Jiao, X. Liu, X. Yin, Y. Si, J. Yu, B. Ding, Antibacterial and antiviral N-halamine nanofibrous membranes with nanonet structure for bioprotective applications, Compos. Commun. 24 (2021) with nanonet, https://doi.org/10.1016/j.coco.2021.100668 100668.

[16] A. Konda, A. Prakash, G.A. Moss, M. Schmoldt, G.D. Grant, S. Guha, Aerosol filtration efficiency of common fabrics used in respiratory cloth masks, ACS Nano 14 (5) (2020) 6339–6347, https://doi.org/10.1021/acsnano.0c03252.

[17] L.H. Kwong, R. Wilson, S. Kumar, Y.S. Crider, Y. Reyes Sanchez, D. Rempel, A. Pillarisetti, Review of the breathability and filtration efficiency of common

[18] W.W.F. Leung, Q. Sun, Electrostatic charged nanofiber filter for filtering airborne novel coronavirus (COVID-19) and nano-aerosols, Sep. Purif. Technol. 250 (2020), https://doi.org/10.1016/j.seppur.2020.116886 116886.

[19] T. Lu, J. Cui, Q. Qu, Y. Wang, J. Zhang, R. Xiong, W. Ma, C. Huang, Multistructured electrospun nanofibers for air filtration: a review, ACS Appl. Mater. Inter. 13 (20) (2021) 23293–23313, https://doi.org/10.1021/acsami.1c06520.

[20] H.K. Kang, H.J. Oh, J.Y. Kim, H.Y. Kim, Y.O. Choi, Effect of process control parameters on the filtration performance of PAN-CTAB nanofiber/nanonet web combined with meltblown nonwoven, Polymers-Basel 13 (20) (2021) 3591, https://doi.org/10.3390/polym13203591.

[21] D.H. Kang, N.K. Kim, H.W. Kang, Electrostatic charge retention in PVDF nanofiber-nylon mesh multilayer structure for effective fine particulate matter filtration for face masks, Polymers-Basel 13 (19) (2021) 3235, https://doi.org/10.3390/polym13193235.

[22] N. Hussain, M. Mehdi, M. Yousif, A. Ali, S. Ullah, S. Hussain Siyal, T. Hussain, I.S. Kim, Synthesis of highly conductive electrospun recycled polyethylene terephthalate nanofibers using the electroless deposition method, Nanomaterials 11 (2) (2021) 531, https://doi.org/10.3390/nano11020531.

[23] J. Zhou, Q. Cai, X. Liu, Y. Ding, F. Xu, Temperature effect on the mechanical properties of electrospun PU nanofibers, Nanoscale Res. Lett. 13 (1) (2018) 384–389, https://doi.org/10.1186/s11671-018-2801-1.

[24] A. Sanyal, S. Sinha-Ray, Ultrafine PVDF nanofibers for filtration of air-borne particulate matters: a comprehensive review, Polymers-Basel 13 (11) (2021) 1864, https://doi.org/10.3390/polym13111864.

[25] Q. Sun, W.W. Leung, Enhanced nano-aerosol loading performance of multilayer PVDF nanofiber electret filters, Sep. Purif. Technol. 240 (2020), https://doi.org/10.1016/j.seppur.2020.116606 116606.

[26] Z. He, F. Rault, M. Lewandowski, E. Mohsenzadeh, F. Salaun, Electrospun PVDF nanofibers for piezoelectric applications: a review of the influence of electrospinning parameters on the beta phase and crystallinity enhancement, Polymers-Basel 13 (2) (2021) 174, https://doi.org/10.3390/polym13020174.

[27] G. Kalimuldina, N. Turdakyn, I. Abay, A. Medeubayev, A. Nurpeissova, D. Adair, Z. Bakenov, A review of piezoelectric PVDF film by electrospinning and its applications, Sensors 20 (18) (2020) 5214, https://doi.org/10.3390/s20185214.

[28] J. Xiong, W. Shao, L. Wang, C. Cui, Y. Gao, Y. Jin, H. Yu, P. Han, F. Liu, J. He, High-performance anti-haze window screen based on multiscale structured polyvinylidene fluoride nanofibers, J. Colloid. Interf. Sci. 607 (2022) 711–719, https://doi.org/10.1016/j.jcis.2021.09.040.

[29] S. Zhang, H. Liu, N. Tang, N. Ali, J. Yu, B. Ding, Highly efficient, transparent, and multifunctional air filters using self-assembled 2D nanoarchitectured fibrous networks, ACS Nano 13 (11) (2019) 13501–13512, https://doi.org/10.1021/acsnano.9b07293.

[30] H. Liu, S. Zhang, L. Liu, J. Yu, B. Ding, High-performance $PM_{0.3}$ air filters using self-polarized electret nanofiber/nets, Adv. Funct. Mater. 30 (13) (2020) 1909554, https://doi.org/10.1002/adfm.201909554.

[31] Y. Si, J. Li, C. Zhao, Y. Deng, Y. Ma, D. Wang, G. Sun, Biocidal and rechargeable N-halamine nanofibrous membranes for highly efficient water disinfection, ACS Biomater Sci Eng. 3 (5) (2017) 854–862, https://doi.org/10.1021/acsbiomaterials.7b00111.

[32] R. He, J. Li, M. Chen, S. Zhang, Y. Cheng, X. Ning, N. Wang, Tailoring moisture electroactive Ag/Zn@cotton coupled with electrospun PVDF/PS nanofibers for antimicrobial face masks, J. Hazard. Mater. 428 (2022), https://doi.org/10.1016/j.jhazmat.2022.128239 128239.

[33] S. Zhang, H. Dong, R. He, N. Wang, Q. Zhao, L. Yang, Z. Qu, L. Sun, S. Chen, J. Ma, J. Li, Hydro electroactive Cu/Zn coated cotton fiber nonwovens for antibacterial and antiviral applications, Int. J. Biol. Macromol. 207 (2022) 100–109, https://doi.org/10.1016/j.ijbiomac.2022.02.155.

[34] K. Chen, S.P. Nikam, Z.K. Zander, Y.-H. Hsu, N.Z. Dreger, M. Cakmak, M.L. Becker, Continuous fabrication of antimicrobial nanofiber mats using post-electrospinning functionalization for roll-to-roll scale-up, ACS Appl. Polym. Mater. 2 (2) (2020) 304–316, https://doi.org/10.1021/acsapm.9b00798.

[35] A. Dong, Y.J. Wang, Y. Gao, T. Gao, G. Gao, Chemical insights into antibacterial N-halamines, Chem. Rev. 117 (6) (2017) 4806–4862, https://doi.org/10.1021/acs.chemrev.6b00687.

[36] F. Wang, L. Huang, P. Zhang, Y. Si, J. Yu, B. Ding, Antibacterial N-halamine fibrous materials, Compos. Commun. 22 (2020), https://doi.org/10.1016/j.coco.2020.100487 100487.

[37] Y.W. Huang, Z.M. Wang, X. Yan, J. Chen, Y.J. Guo, W.Z. Lang, Versatile polyvinylidene fluoride hybrid ultrafiltration membranes with superior antifouling, antibacterial and self-cleaning properties for water treatment, Colloid. Interf. Sci. 505 (2017) 38–48, https://doi.org/10.1016/j.jcis.2017.05.076.

[38] C.H. Cheng, H.C. Liu, J.C. Lin, Surface modification of polyurethane membrane with various hydrophilic monomers and N-halamine: surface characterization and antimicrobial properties evaluation, Polymers-Basel 13 (14) (2021) 2321, https://doi.org/10.3390/polym13142321.

[39] M. Liang, F. Wang, M. Liu, J. Yu, Y. Si, B. Ding, N-halamine functionalized electrospun poly(vinyl alcohol-co-ethylene) nanofibrous membranes with rechargeable antibacterial activity for bioprotective applications, Adv. Fiber Mater. 1 (2) (2019) 126–136, https://doi.org/10.1007/s42765-019-00008-9.

[40] H. Wang, Z.M. Wang, X. Yan, J. Chen, W.Z. Lang, Y.J. Guo, Novel organic-inorganic hybrid polyvinylidene fluoride ultrafiltration membranes with

antifouling and antibacterial properties by embedding N-halamine functionalized silica nanospheres, J. Ind. Eng. Chem. 52 (2017) 295–304, https://doi.org/10.1016/j.jiec.2017.03.059.

[41] P. Capkova, M. Kormunda, Z. Kolska, J. Trögl, M. Munzarova, P. Rysanek, Electrospun antimicrobial PVDF-DTAB nanofibrous membrane for air filtration: effect of DTAB on structure, morphology, adhesion, and antibacterial properties, Macromol. Mater. Eng. 303 (3) (2018) 1700415, https://doi.org/10.1002/mame.201700415.

[42] Z.C. Xiong, R.L. Yang, Y.J. Zhu, F.F. Chen, L.Y. Dong, Flexible hydroxyapatite ultralong nanowire-based paper for highly efficient and multifunctional air filtration, J. Mater. Chem. 5 (33) (2017) 17482–17491, https://doi.org/10.1039/c7ta03870d.

[43] A. Lakshmanan, D.S. Gavali, R. Thapa, D. Sarkar, Synthesis of CTAB-functionalized large-scale nanofibers air filter media for efficient PM$_{2.5}$ Capture capacity with low airflow resistance, ACS Appl. Polym. Mater. 3 (2) (2021) 937–948, doi: 10.1021/acsapm.0c01203.

[44] C. Huang, Y. Chen, G. Sun, K. Yan, Disinfectant performance of a chlorine regenerable antibacterial microfiber fabric as a reusable wiper, Materials 12 (1) (2019) 127, https://doi.org/10.3390/ma12010127.

[45] S. Kumar, J. Jang, H. Oh, B. J. Jung, Y. Lee, H. Park, K.H. Yang, Y. Chang Seong, J.-S. Lee, Antibacterial polymeric nanofibers from zwitterionic terpolymers by electrospinning for air filtration, ACS Appl. Nano. Mater. 4 (3) (2020) 2375–2385, doi: 10.1021/acsanm.0c02366.

[46] Z. Xia, H. Liu, S. Wang, Z. Meng, N. Ren, Preparation and dechlorination of a poly(vinylidene difluoride)-grafted acrylic acid film immobilized with Pd/Fe bimetallic nanoparticles for monochloroacetic acid, Chem. Eng. J. 200–202 (2012) 214–223, https://doi.org/10.1016/j.cej.2012.06.056.

[47] R. Li, M. Sun, Z. Jiang, X. Ren, T.S. Huang, N-halamine-bonded cotton fabric with antimicrobial and easy-care properties, Fiber. Polym. 15 (2) (2014) 234–240, https://doi.org/10.1007/s12221-014-0234-8.

[48] X. Ren, H.B. Kocer, S.D. Worley, R.M. Broughton, T.S. Huang, Rechargeable biocidal cellulose: Synthesis and application of 3-(2,3-dihydroxypropyl)-5,5-dimethylimidazolidine-2,4-dione, Carbohydr. Polym. 75 (4) (2009) 683–687, https://doi.org/10.1016/j.carbpol.2008.09.012.

[49] X. Ren, L. Kou, H.B. Kocer, C. Zhu, S.D. Worley, R.M. Broughton, T.S. Huang, Antimicrobial coating of an N-halamine biocidal monomer on cotton fibers via admicellar polymerization, Colloid. Surface. A. 317 (1–3) (2008) 711–716, https://doi.org/10.1016/j.colsurfa.2007.12.007.

[50] C. Liu, H. Shan, X. Chen, Y. Si, X. Yin, J. Yu, B. Ding, Novel inorganic-based N-halamine nanofibrous membranes as highly effective antibacterial agent for water disinfection, ACS. Appl. Mater. 10 (51) (2018) 44209–44215, https://doi.org/10.1021/acsami.8b18322.

[51] Y. Liu, J. Li, X. Cheng, X. Ren, T.S. Huang, Self-assembled antibacterial coating by N-halamine polyelectrolytes on a cellulose substrate, J. Mater. Chem. B. 3 (7) (2015) 1446–1454, https://doi.org/10.1039/c4tb01699h.

[52] W.W.F. Leung, C.H. Hung, P.T. Yuen, Effect of face velocity, nanofiber packing density and thickness on filtration performance of filters with nanofibers coated on a substrate, Gas Sep. Purif. 71 (1) (2010) 30–37, https://doi.org/10.1016/j.seppur.2009.10.017.

[53] F. Wang, M. Liu, R. Ding, M. Liang, L. Huang, J. Yu, Y. Si, Rechargeable antibacterial polysulfonamide-based N-halamine nanofibrous membranes for bioprotective applications, ACS Appl. Bio Mater. 2 (8) (2019) 3668–3677, https://doi.org/10.1021/acsabm.9b00537.

[54] M.M. Mahmud, S. Zaman, A. Perveen, R.A. Jahan, M.F. Islam, M.T. Arafat, Controlled release of curcumin from electrospun fiber mats with antibacterial activity, J. Drug Delivery Sci. Technol. 55 (2020), https://doi.org/10.1016/j.jddst.2019.101386 101386.

[55] D. Kharaghani, Y. Kee Jo, M.Q. Khan, Y. Jeong, H.J. Cha, I.S. Kim, Electrospun antibacterial polyacrylonitrile nanofiber membranes functionalized with silver nanoparticles by a facile wetting method, Eur. Polym. J. 108 (2018) 69–75, https://doi.org/10.1016/j.eurpolymj.2018.08.021.

[56] G. Kasi, S. Gnanasekar, K. Zhang, E.T. Kang, L.Q. Xu, Polyurethane-based composites with promising antibacterial properties, J. Appl. Polym. Sci. 139 (20) (2022) 52181, https://doi.org/10.1002/app.52181.